Quantitative Imaging of Nitrogen Fixation by Individual Bacteria Within Animal Cells

Claude P. Lechene, *et al.*

Science **317**, 1563 (2007);
DOI: 10.1126/science.1145557

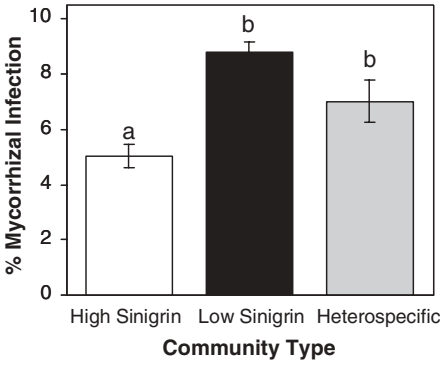

Fig. 5. Mycorrhizal infection potential (measured as the percentage of root sections colonized with mycorrhizal fungus) in soil from high- and low-sinigrin *B. nigra* communities and mixed heterospecific communities (means ± SE). Bars sharing the same letters are not statistically different.

Plants in the Brassicaceae are characteristically nonmycorrhizal, whereas we observed that the three heterospecific competitors, like almost all other angiosperms, do form mutualistic associations with mycorrhizal fungi. Therefore, the observed pattern in MIP among community types may explain the pattern of lower fitness of heterospecifics in high-sinigrin *B. nigra* communities and higher fitness of high-sinigrin *B. nigra* invaders in heterospecific communities. The higher fitness of low-sinigrin *B. nigra* invaders in *B. nigra* monocultures is consistent with a cost of sinigrin production (*22*) and little benefit of high sinigrin levels when competing with nonmycorrhizal *B. nigra* neighbors. Other mechanisms, such as direct allelopathy, may be acting as well (*23*).

Our field data show an intransitive competitive hierarchy between competing species and genotypes leading to cyclical dynamics; high-sinigrin *B. nigra* can invade diverse communities of other species, low-sinigrin *B. nigra* can invade patches of high-sinigrin *B. nigra*, and other species can invade patches of low-sinigrin *B. nigra*. Thus, each species or genotype is able to invade at least one other community type, promoting coexistence through mutual invasibility (*19*). For instance, a diverse, heterospecific community could be invaded by high-sinigrin genotypes of *B. nigra*. As *B. nigra* rises in abundance, displacing heterospecifics, selection will begin to favor lower-sinigrin concentrations. If sinigrin concentrations fall low enough, heterospecific species may be able to reinvade the community, starting the cycle over. This kind of "rock-paper-scissors" intransitivity has been shown to allow coexistence between species (*24*, *25*) and genotypes within species (*26*, *27*), but few studies have investigated intransitive networks consisting of different species and genotypes within one species (*28*)

The experimental results, combined with natural observations, show that in this system, the maintenance of species diversity is dependent on sufficient genetic variation, because without this variation the system would become dominated by *B. nigra* (if sinigrin levels are uniformly high), or by other species (if sinigrin levels are uniformly low). Simultaneously, the maintenance of genetic variation is dependent on species diversity, because selection is predicted to fix sinigrin levels at their lowest level if other competing species are not present. Our experiments show that a trade-off between intra- and interspecific competitive ability in the genetically variable species led to an intransitive competitive hierarchy among competing species and genotypes, thereby promoting coexistence. These results clearly show the potential for genetic variability and microevolution within species to alter community dynamics and structure. Conservation efforts aimed at maintaining species diversity therefore should not overlook the potential impacts of losses of genetic diversity, which could ultimately lead to losses of interacting species.

References and Notes

1. D. Tilman, *Resource Competition and Community Structure* (Princeton Univ. Press, Princeton, NJ, 1982).
2. R. D. Holt, J. Grover, D. Tilman, *Am. Nat.* **144**, 741 (1994).
3. P. Chesson, *Annu. Rev. Ecol. Syst.* **31**, 343 (2000).
4. M. Kimura, *The Neutral Theory of Molecular Evolution* (Cambridge Univ. Press, Cambridge, 1983).
5. M. G. Bulmer, *Genome* **31**, 761 (1989).
6. D. S. Falconer, T. F. C. MacKay, *Introduction to Quantitative Genetics* (Longman Group, Essex, UK, 1996).
7. T. G. Whitham *et al.*, *Ecology* **84**, 559 (2003).
8. G. M. Crutsinger *et al.*, *Science* **313**, 966 (2006).
9. M. T. J. Johnson, M. J. Lajeunesse, A. A. Agrawal, *Ecol. Lett.* **9**, 24 (2006).
10. P. A. Abrams, *Evol. Int. J. Org. Evol.* **60**, 427 (2006).
11. M. Vellend, *Ecology* **87**, 304 (2006).
12. S. Y. Strauss, R. E. Irwin, *Ann. Rev. Ecol. Evol. System.* **35**, 435 (2004).
13. R. P. Schreiner, R. T. Koide, *New Phytol.* **123**, 107 (1993).
14. A. F. Raybould, C. L. Moyes, *Heredity* **87**, 383 (2001).
15. D. J. Kliebenstein, *Plant Cell Environ.* **27**, 675 (2004).
16. P. Feeny, L. Rosenberry, *Biochem. Syst. Ecol.* **10**, 23 (1982).
17. M. B. Traw, *Evol. Int. J. Org. Evol.* **56**, 2196 (2002).
18. Materials and methods are available as supporting material on *Science* Online.
19. P. L. Chesson, S. Ellner, *J. Math. Biol.* **27**, 117 (1989).
20. K. A. Stinson *et al.*, *PLoS Biol.* **4**, 727 (2006).
21. M. Giovannetti, B. Mosse, *New Phytol.* **84**, 489 (1980).
22. R. Mauricio, M. D. Rausher, *Evol. Int. J. Org. Evol.* **51**, 1435 (1997).
23. D. H. Siemens, S. H. Garner, T. Mitchell-Olds, R. M. Callaway, *Ecology* **83**, 505 (2002).
24. L. W. Buss, J. B. C. Jackson, *Am. Nat.* **113**, 223 (1979).
25. R. A. Laird, B. S. Schamp, *Am. Nat.* **168**, 182 (2006).
26. B. Sinervo, C. M. Lively, *Nature* **380**, 240 (1996).
27. B. Kerr, M. A. Riley, M. W. Feldman, B. J. M. Bohannan, *Nature* **418**, 171 (2002).
28. D. R. Taylor, L. W. Aarssen, *Am. Nat.* **136**, 305 (1990).

29. We thank R. Karban, M. L. Stanton, and three anonymous reviewers for comments, D. Kliebenstein for assistance with and equipment for chemical analysis, A. E. Bennett for assistance in assaying mycorrhizal infection potential, the members of the Strauss lab group for discussions of experimental design, and Z. Costa and O. Ervin for assistance with fieldwork. This work was supported by a NSF Graduate Research Fellowship (to R.A.L.), the U.C. Agricultural Experiment Station (S.Y.S.), U.C. Davis, and an NSF Doctoral Dissertation Improvement Grant (to R.A.L. and S.Y.S.).

Supporting Online Material

www.sciencemag.org/cgi/content/full/317/5844/1561/DC1
Materials and Methods
References

6 July 2007; accepted 25 July 2007
10.1126/science.1147455

Quantitative Imaging of Nitrogen Fixation by Individual Bacteria Within Animal Cells

Claude P. Lechene,[1]* Yvette Luyten,[2]† Gregory McMahon,[1] Daniel L. Distel[2]*

Biological nitrogen fixation, the conversion of atmospheric nitrogen to ammonia for biosynthesis, is exclusively performed by a few bacteria and archaea. Despite the essential importance of biological nitrogen fixation, it has been impossible to quantify the incorporation of nitrogen by individual bacteria or to map the fate of fixed nitrogen in host cells. In this study, with multi-isotope imaging mass spectrometry we directly imaged and measured nitrogen fixation by individual bacteria within eukaryotic host cells and demonstrated that fixed nitrogen is used for host metabolism. This approach introduces a powerful way to study microbes and global nutrient cycles.

Bacteria and archaea responsible for biological nitrogen fixation can be found in free-living form (*1*–*3*) or in symbiosis with algae (*4*, *5*), higher plants (*3*, *5*), and some animals (*6*–*8*). Although these microbes are a critical part of the global nitrogen cycle (*9*), there has previously been no means to evaluate this fixation process at subcellular resolution. This is now possible with multi-isotope imaging mass spectrometry (MIMS) (*10*).

Wood and woody plant materials are abundant in the biosphere (*11*) and are important nutrient sources for a variety of fungi and microorganisms (*12*). Yet few animals are able to feed primarily on wood (*13*). Although rich in carbon, wood typically contains two orders of

magnitude less nitrogen per unit of carbon than does animal tissue (*14*). Animals using wood as food must therefore obtain other sources of combined nitrogen for biosynthesis. For example, wood-eating termites are thought to supplement their diet with nitrogenous compounds produced by nitrogen-fixing bacteria inhabiting their gut (*6*). This conclusion is supported by observations that a variety of nitrogen-fixing bacteria have been cultivated from termite guts (*11*) or detected by culture-independent methods (*15*, *16*), and that substantial rates of nitrogen fixation have been measured in association with termite guts and intact termite colonies (*6*). Direct measurement of nitrogen fixation by individual bacteria and of nitrogen use by host cells, however, has remained impossible.

Nitrogen fixation has also been detected in intact specimens of wood-eating marine bivalves of the family Teredinidae (commonly known as shipworms) (*17*), but the site of fixation and the identity of the nitrogen-fixing microorganisms have not been previously determined. Although conspicuous communities of nitrogen-fixing bacteria have not been found in the gut of shipworms (*13*), as they have in termites, dense populations of intracellular bacterial symbionts have been observed in cells (bacteriocytes) in a region of shipworm gills known as the gland of Deshayes (*18*). Moreover, a bacterium (*Teredinibacter turnerae*) capable of fixing nitrogen gas (N_2) in pure culture has been isolated from the gills of numerous shipworm species (*19*, *20*), and its presence in the gill symbiont community of the shipworm *Lyrodus pedicellatus* has been confirmed by in situ hybridization and quantitative polymerase chain reaction analysis (*21*–*23*). These observations raise the questions of whether bacterial symbionts within the gills of *L. pedicellatus* can fix nitrogen and whether this fixed nitrogen is supplied to the host.

We localized and measured nitrogen fixation by individual cells of *T. turnerae* in pure culture, by individual bacterial symbionts in the gill of *L. pedicellatus*, and in subcellular domains of bacteria-free host tissue, using MIMS (*10*) to measure the incorporation of nitrogen gas enriched in the rare stable isotope ^{15}N. With MIMS methodology, quantitative mass images (QMIs) were generated (and the isotope values derived) by quantifying light and heavy isotopes of secondary cyanide ions ($^{12}C^{14}N^-$ and $^{12}C^{15}N^-$) produced by bombardment of the tissue with a primary cesium ion beam (*10*). The tissue was visualized by mapping the distribution of the naturally abundant isotope ^{14}N (as represented by $^{12}C^{14}N^-$) to produce a high-resolution image of nitrogen-containing tissue. A second image, simultaneously acquired in parallel, mapped the distribution of the rare isotope ^{15}N (as represented by $^{12}C^{15}N^-$) (*24*). The incorporation of ^{15}N tracer could then be measured by comparing the two quantitative images to determine the increase of $^{15}N/^{14}N$ ratios as compared to the natural abundance ratio (0.00367). We represented the enrichment of ^{15}N in tissue using a color-coded transform [hue saturation intensity (HSI)] of the isotope ratio values (*10*, *25*).

We first established that MIMS could be used to measure nitrogen fixation by individual cells of *T. turnerae* grown in axenic culture in vitro (*24*). When grown in the presence of $^{15}N_2$ tracer (without a combined nitrogen source in the medium), biological nitrogen fixation could be detected as a time-dependent increase in the $^{15}N/^{14}N$ isotope ratio in individual bacteria. In cultured *T. turnerae*, we found that the mean ^{15}N fraction increased by a factor of 7 to 9 over its natural ratio after 30 min, by a factor of 20 to 28 after 8 hours, and by a factor of 68 after 7 days (Fig. 1, A to C). There was no detectable elevation of the $^{15}N/^{14}N$ ratio in cells of *Enterococcus faecalis*, a bacterium lacking the ability to fix nitrogen, when grown for the same estimated number of generations in the presence of the $^{15}N_2$ tracer and analyzed together with *T. turnerae* in a mixed population (Fig. 1, A to C).

We then applied MIMS to measure the incorporation of ^{15}N by symbionts within gill bacteriocytes in vivo by exposing *L. pedicellatus* to ^{15}N-labeled N_2 while in their intact wood burrows (*24*). After 8 days of exposure, there was a dramatic elevation of the $^{15}N/^{14}N$ ratio in localized regions within the gland of Deshayes, demonstrating the incorporation of gaseous $^{15}N_2$ into the molecular makeup of these regions (Figs. 1D and 2, A to I, and supporting online text). The $^{12}C^{14}N$ QMIs (*10*) showed that these regions appeared to contain densely packed bacteria. We measured nitrogen fixation by thousands of

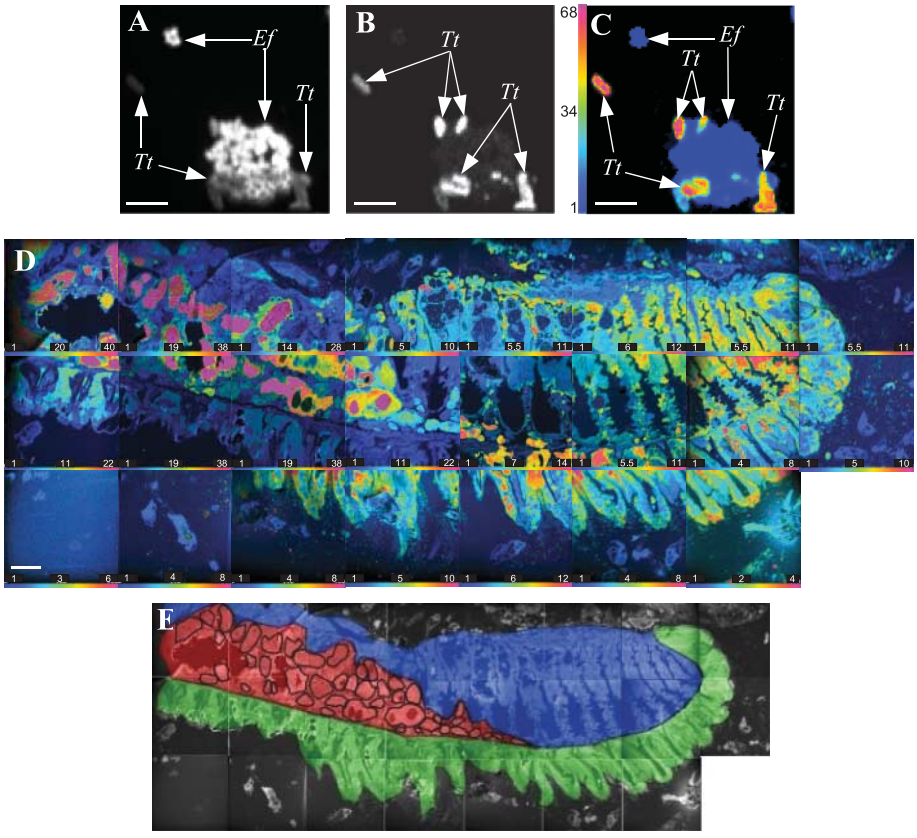

Fig. 1. N fixation by isolated *T. turnerae* bacteria and by bacterial symbionts within the marine bivalve *L. pedicellatus*. (**A** and **B**) Parallel QMIs of one field containing *T. turnerae* (*Tt*) and *E. faecalis* (*Ef*). (A) $^{12}C^{14}N^-$. (B) $^{12}C^{15}N^-$. (**C**) HSI of the ratio (B)/(A). The image is 256 × 256 pixels; acquisition time was 30 min. Scale bar, 5 μm. (**D**) Mosaic of HSI of the $^{12}C^{15}N/^{12}C^{14}N$ ratio from *L. pedicellatus*. Each tile is 100 × 100 μm and 256 × 256 pixels; acquisition time was 120 min per tile. Scale bar, 25 μm. The HSI scales represent the measured $^{15}N/^{14}N$ ratio divided by the natural abundance ratio. The scale ranges from blue (denoting a factor of 1; that is, the natural value) to magenta (denoting an increase over the natural value by at least the factor indicated on the right of each bar). (**E**) Cartoon of (D), outlining the location of the gland of Deshayes (red), interlamellar junctions (blue), ctenidial filaments (green), and bacteriocytes (outlines). In (C), the highest ^{15}N incorporation is seen in *T. turnerae* and none in *E. faecalis* . In (D), the highest ^{15}N incorporation is seen in bacteriocytes of the gland of Deshayes.

[1]National Resource for Imaging Mass Spectrometry, Harvard Medical School, and Brigham and Women's Hospital, 65 Landsdowne Street, Cambridge, MA 02139, USA. [2]Ocean Genome Legacy, Center for Marine Genomic Research, 240 County Road, Ipswich, MA 01938-2723, USA.

*To whom correspondence should be addressed. E-mail: cpl@harvard.edu (C.P.L.); distel@oglf.org (D.L.D.)

†Present address: New England Biolabs, 240 County Road, Ipswich, MA 01938-2723, USA.

individual symbiotic bacteria. The values of $^{15}N/^{14}N$ ranged from a factor of 17 to a factor of 68 over the natural ratio, with a mean increase of a factor of 39 (Fig. 4A, Table 1, and supporting online text). Furthermore, we were able to successively image the same gill tissue sections, first with transmission electron microscopy (TEM) and then MIMS. The images produced by the two methods could be precisely superimposed, confirming the identity of the densely packed bacteria observed in the MIMS images (Fig. 2, G to I). This enabled us to find that the regions immediately adjacent to the periphery of individual bacteria had a degree of ^{15}N incorporation that was slightly more elevated (but with high statistical significance) than that within the bacteria (supporting online text). These results demonstrate that nitrogen is fixed by endosymbiotic bacteria within the gills of *L. pedicellatus* and suggest that molecules containing fixed nitrogen are transported to the proximity of the bacterial cell surface. The variation in ^{15}N fixation among individual bacteria could reflect differences in the physiological state of symbionts or genetic differences among symbionts within individual bacteriocytes. The latter is consistent with previous observations indicating the co-existence of multiple symbiont ribotypes within individual bacteriocytes in *L. pedicellatus (22)*. The variation could reflect bacteriocytes at different stages of development (*26*).

The $^{15}N/^{14}N$ ratios were also elevated in gill regions and structures that were free of bacteria, such as in discrete cells located at the base of the gill filaments and in individual cilia in the gill apex where new filaments are formed (Fig. 3, A to C and E to J). We circumscribed hundreds of subcellular regions of interest (ROIs) on these structures and found increased $^{15}N/^{14}N$ values ranging from a factor of 1.4 to a factor of 11 over the natural ratio, with a mean increase of a factor of 5 for ROIs in both the ctenidial (gill) filaments and interlamellar junctions (Fig. 4A, Table 1, and supporting online text). We confirmed the absence of symbionts in these ROIs by TEM analysis (Fig. 3D). Although ^{15}N was incorporated in symbiont-free regions, the highest values in these regions were lower than the minimum value measured in the symbiotic bacteria (Fig. 4A and Table 1). The observed distribution of ^{15}N incorporation (high in symbionts, low in symbiont-free cells) is consistent with the transfer of newly fixed nitrogen from its source in symbionts to its inclusion in host cellular pools. These results provide strong evidence that newly fixed nitrogen is used by shipworm cells for biosynthesis (Fig. 4B).

MIMS technology has allowed us to localize, quantify, and compare nitrogen fixation in single cells and subcellular structures. We have demonstrated nitrogen fixation by individual symbiotic bacteria and have provided strong evidence of its use by the host. This symbiotic strategy is reminiscent of symbioses proposed to occur in the root nodules of leguminous plants and may explain the unusual ability of *L. pedicellatus* to

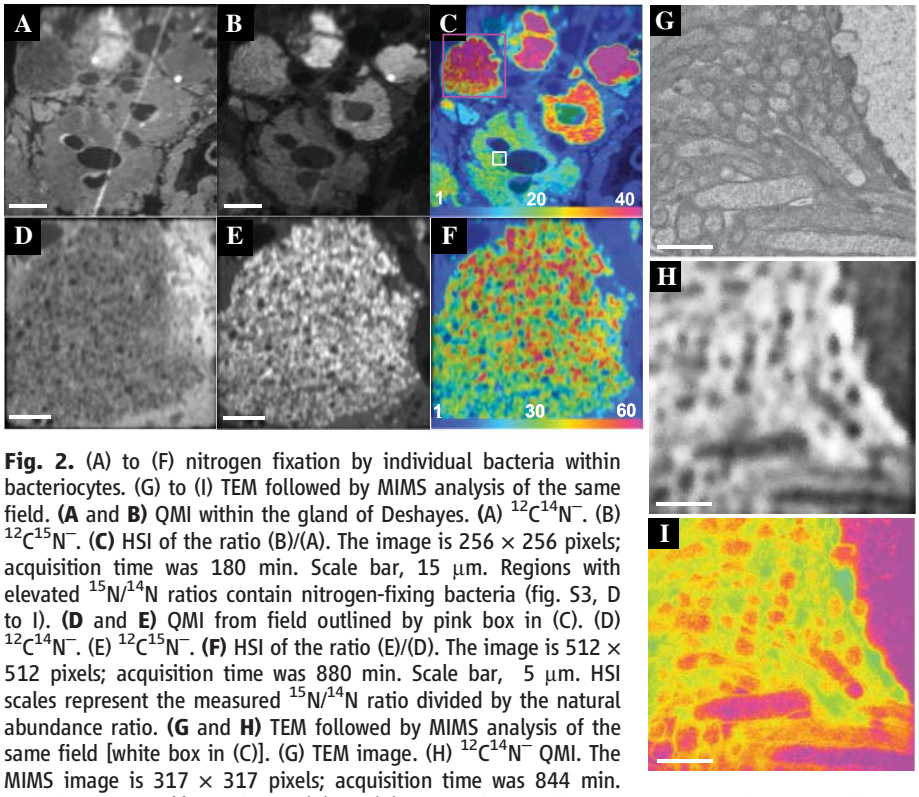

Fig. 2. (A) to (F) nitrogen fixation by individual bacteria within bacteriocytes. (G) to (I) TEM followed by MIMS analysis of the same field. **(A** and **B)** QMI within the gland of Deshayes. (A) $^{12}C^{14}N^-$. (B) $^{12}C^{15}N^-$. **(C)** HSI of the ratio (B)/(A). The image is 256 × 256 pixels; acquisition time was 180 min. Scale bar, 15 μm. Regions with elevated $^{15}N/^{14}N$ ratios contain nitrogen-fixing bacteria (fig. S3, D to I). **(D** and **E)** QMI from field outlined by pink box in (C). (D) $^{12}C^{14}N^-$. (E) $^{12}C^{15}N^-$. **(F)** HSI of the ratio (E)/(D). The image is 512 × 512 pixels; acquisition time was 880 min. Scale bar, 5 μm. HSI scales represent the measured $^{15}N/^{14}N$ ratio divided by the natural abundance ratio. **(G** and **H)** TEM followed by MIMS analysis of the same field [white box in (C)]. (G) TEM image. (H) $^{12}C^{14}N^-$ QMI. The MIMS image is 317 × 317 pixels; acquisition time was 844 min. Scale bar, 1 μm. **(I)** Overlay of (G) on (H). Note the excellent registration of the TEM and MIMS images.

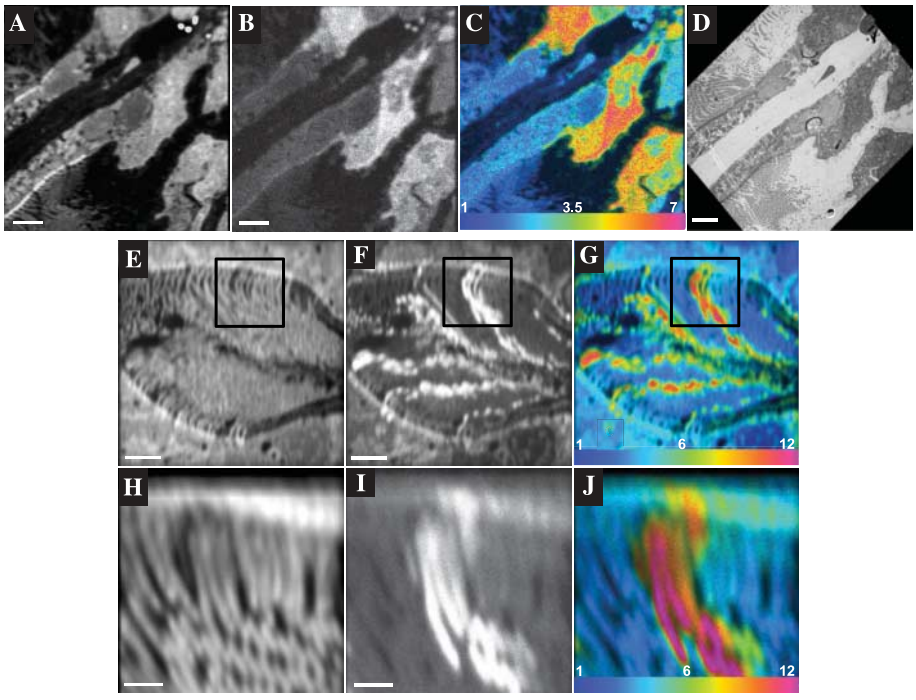

Fig. 3. Newly fixed nitrogen in bacteria-free regions of *L. pedicellatus*. **(A** and **B)** QMI of a ctenidial filament. (A) $^{12}C^{14}N^-$. (B) $^{12}C^{15}N^-$. **(C)** HSI of the ratio (B)/(A). The image is 256 × 256 pixels; acquisition time was 200 min. Scale bar, 5 μm. **(D)** TEM of a section consecutive to (A) to (C). Scale bar, 5 μm. **(E** and **F)** QMI of a lateral cilium. (E) $^{12}C^{14}N^-$. (F) $^{12}C^{15}N^-$. **(G)** HSI of the ratio (F)/(E). The image is 512 × 512 pixels; acquisition time was 880 min. Scale bar, 3 μm. **(H** and **I)** QMI of the area boxed in (E) to (G). (H) $^{12}C^{14}N^-$. (I) $^{12}C^{15}N^-$. **(J)** HSI of the ratio (I)/(H). The image is 512 × 512 pixels; acquisition time was 880 min. Scale bar, 1 μm. HSI scales represent the measured $^{15}N/^{14}N$ ratio divided by the natural abundance ratio. Note the elevated $^{12}C^{15}N/^{12}C^{14}N$ ratios in bacteria-free cells and cilia.

Table 1. ^{15}N incorporation in *L. pedicellatus* expressed as the experimental/terrestrial $^{15}N/^{14}N$ ratio.

	N	Mean	SD	Maximum	Minimum
Bacteria within bacteriocytes	1863	39.1	11.9	67.9	17.1
Ctenidial filaments	254	5.44	2.67	11.0	1.39
Interlamellar junctions	152	5.31	2.02	9.81	1.53

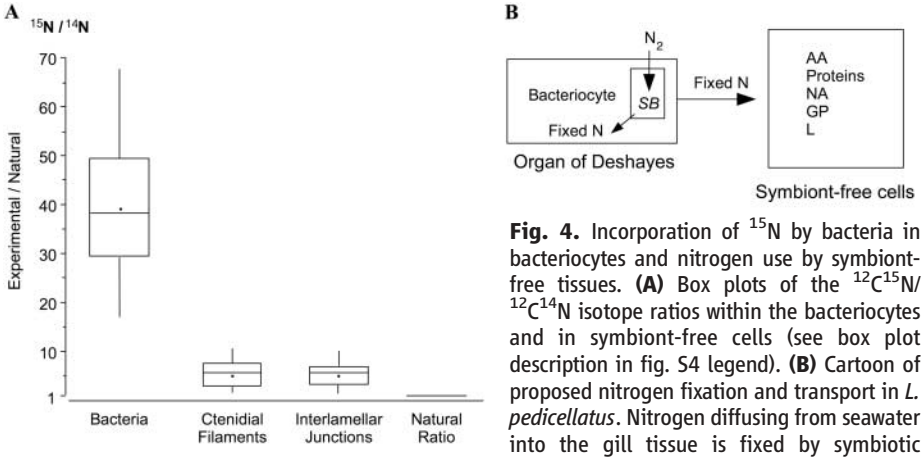

Fig. 4. Incorporation of ^{15}N by bacteria in bacteriocytes and nitrogen use by symbiont-free tissues. **(A)** Box plots of the $^{12}C^{15}N/^{12}C^{14}N$ isotope ratios within the bacteriocytes and in symbiont-free cells (see box plot description in fig. S4 legend). **(B)** Cartoon of proposed nitrogen fixation and transport in *L. pedicellatus*. Nitrogen diffusing from seawater into the gill tissue is fixed by symbiotic bacteria (*SB*) in the gland of Deshayes, then transported away and diluted into the host's biomass pool, providing nitrogen for synthesis of amino acids (AA), proteins, nucleic acids (NA), glycoproteins (GP), and compound lipids (L) used for host tissue metabolism.

survive and grow on a nearly nitrogen-free diet of wood (*27*) (Fig. 4B). Thus, this work suggests a function for the shipworm/bacteria symbiosis that has not been demonstrated previously for any other animal endosymbiosis: the conversion of nitrogen from atmospheric gas into animal biomass. This method, which also can be applied to measure the distribution of any stable (or radioactive) isotope-labeled molecule at micrometer to nanometer scales, provides a template for the study of individual microbes in a population and of their roles in the physiology, pathology, and ecology of life.

References and Notes

1. *Genetics and Regulation of Nitrogen Fixation in Free-Living Bacteria* (Kluwer Academic, Dordrecht, Netherlands, 2004).
2. J. P. Zehr, E. J. Carpenter, T. A. Villareal, *Trends Microbiol.* **8**, 68 (2000).
3. C. C. Cleveland *et al.*, *Global Biogeochem. Cycles* **13**, 623 (1999).
4. T. A. Villareal, in *Marine Pelagic Cyanobacteria: Trichodesmium and Other Diazotrophs*, E. Carpenter, D. Capone, J. Rueter, Eds. (Kluwer Academic, Dordrecht, Netherlands, 1992), pp. 163–175.
5. A. Rai, E. Soderback, B. Bergman, *New Phytol.* **147**, 449 (2000).
6. J. A. Breznak, in *Termites: Evolution, Sociality, Symbioses, Ecology*, T. Abe, D. E. Bignell, M. M. Higashi, Eds. (Kluwer Academic, Dordrecht, Netherlands, 2000), pp. 209–232.
7. J. B. Nardi, R. I. Mackie, J. O. Dawson, *J. Insect Physiol.* **48**, 751 (2002).
8. M. P. Lesser, C. H. Mazel, M. Y. Gorbunov, P. G. Falkowski, *Science* **305**, 997 (2004).
9. E. F. DeLong, D. M. Karl, *Nature* **437**, 336 (2005).
10. C. Lechene *et al.*, *J. Biol.* **5**, 20 (2006).
11. J. A. Breznak, A. Brune, *Annu. Rev. Entomol.* **39**, 453 (1994).
12. G. Daniel, in *Wood Deterioration and Preservation: Advances in Our Changing World*, B. Goodell, D. Nicholas, T. Schultz, Eds. (American Chemical Society, Washington, DC, 2003), pp. 34–72.
13. D. L. Distel, in *Wood Deterioration and Preservation: Advances in Our Changing World*, B. Goodell, D. Nicholas, T. Schultz, Eds. (American Chemical Society, Washington, DC, 2003), pp. 253–271.
14. R. Rynk *et al.*, *On-Farm Composting Handbook* (Northeast Regional Agricultural Engineering Service, Ithaca, NY, 1992).
15. S. Noda, M. Ohkuma, R. Usami, K. Horikoshi, T. Kudo, *Appl. Environ. Microbiol.* **65**, 4935 (1999).
16. M. Ohkuma, S. Noda, T. Kudo, *Appl. Environ. Microbiol.* **65**, 4926 (1999).
17. E. J. Carpenter, J. L. Culliney, *Science* **187**, 551 (1975).
18. J. Popham, M. Dickson, *Mar. Biol.* **19**, 338 (1973).
19. J. B. Waterbury, C. B. Calloway, R. D. Turner, *Science* **221**, 1401 (1983).
20. D. L. Distel, W. Morrill, N. MacLaren-Toussaint, D. Franks, J. Waterbury, *Int. J. Syst. Evol. Microbiol.* **52**, 2261 (2002).
21. D. L. Distel, E. F. DeLong, J. B. Waterbury, *Appl. Environ. Microbiol.* **57**, 2376 (1991).
22. D. L. Distel, D. J. Beaudoin, W. Morrill, *Appl. Environ. Microbiol.* **68**, 6292 (2002).
23. Y. A. Luyten, J. R. Thompson, W. Morrill, M. F. Polz, D. L. Distel, *Appl. Environ. Microbiol.* **72**, 412 (2006).
24. Materials and methods are available as supporting material on *Science* Online
25. G. McMahon, B. J. Glassner, C. P. Lechene, *Appl. Surf. Sci.* **252**, 6895 (2006).
26. C. Fisher, *Rev. Aquat. Sci.* **2**, 399 (1990).
27. S. Gallager, R. Turner, C. Berg, *J. Exp. Mar. Biol. Ecol.* **52**, 63 (1981).

28. This work was supported by an NIH P41 EB001974 grant (to C.P.L.) and an NSF OCE-0425795 grant (to D.L.D.).

Supporting Online Material

www.sciencemag.org/cgi/content/full/317/5844/1563/DC1
Materials and Methods
SOM Text
Figs. S1 to S5
Table S1
References

23 May 2007; accepted 27 July 2007
10.1126/science.1145557